

Article

# One-Pot Aqueous and Template-Free Synthesis of Mesoporous Polymeric Resins

Mahboubeh Nabavinia <sup>1</sup>, Baishali Kanjilal <sup>1</sup>, Alexander Hesketh <sup>1</sup>, Philip Wall <sup>1</sup>, Alireza Shirazi Amin <sup>2</sup>, Peter Kerns <sup>2</sup>, Joseph F. Stanzione III <sup>1</sup>, Steven Suib <sup>2</sup>, Fujian Liu <sup>3,\*</sup> and Iman Noshadi <sup>1,\*</sup>

- <sup>1</sup> Department of Chemical Engineering, Rowan University, Glassboro, NJ 08028, USA; mahboobehnabavi@gmail.com (M.N.); kanjilal.baishali@gmail.com (B.K.); hesketha4@students.rowan.edu (A.H.); wallp8@students.rowan.edu (P.W.); stanzione@rowan.edu (J.F.S.III)
- <sup>2</sup> Department of Chemistry, University of Connecticut, Storrs, CT 06268, USA; alireza.shirazi\_amin@uconn.edu (A.S.A.); Peter.kerns@uconn.edu (P.K.); Steven.suib@uconn.edu (S.S.)
- <sup>3</sup> National Engineering Research Center of Chemical Fertilizer Catalyst (NERC-CFC), School of Chemical Engineering, Fuzhou University, Gongye Street 523, Fuzhou 350002, China
- \* Correspondence: liufujian1982@163.com (F.L.); Noshadi@rowan.edu (I.N.)

Received: 14 August 2019; Accepted: 10 September 2019; Published: 19 September 2019



**Abstract:** This work explores the novel one-pot aqueous phase synthesis of mesoporous phenolic-hyperbranched polyethyleneimine resins without the use of a template, and their utility as heterogeneous catalysts in batch reactors and continuous microreactors. Catalyst surface areas of up to 432 m<sup>2</sup>/g were achieved with a uniform Pd distribution and an interconnected, highly porous, network structure, confirmed through Brunauer–Emmett–Teller (BET) surface area measurements, scanning electron microscopes (SEM), X-Ray Photoelectron Spectroscopy (XPS), Transmission Electron Microscopy (TEM), and Energy-dispersive X-ray spectroscopy (EDS). The heterogeneous catalysts achieved a maximum 98.98 ± 1% conversion in batch Suzuki couplings, with conversions being dependent upon reaction conditions, reactant chemistries, Pd loading and catalyst surface area. The catalysts were shown to be recyclable with only a marginal loss in conversion achieved after five runs. Up to 62 ± 5% and 46.5 ± 8% conversions at 0.2 mL/s and 0.4 mL/s flow rates, respectively, were achieved in a continuous microreactor. Understanding the mechanism of action of this mesoporous resin is a future research area, which could help expand the application vistas for this catalyst platform.

**Keywords:** mesoporous polymers; heterogeneous catalysis; cross-coupling; microreactor

## 1. Introduction

Research interest in the subject of mesoporous polymeric resins (MPRs) is ongoing and extensive, with their applications spanning selective adsorption and water treatment, separation and insulation, and the field of heterogeneous catalysis [1–12]. MPRs proffer intrinsic characteristics such as tunable structures with tailorable mesopores size (2–30 nm) [13–21]. These are distinct advantages when compared to porous organic polymers entailing crystalline covalent organic or aromatic frameworks, conjugated microporous polymers or mesoporous polydivinylbenzene. The active sites in MPRs' structures are more accessible to substrates and hence provide superior catalytic activity. MPRs can be directly carbonized to ordered mesoporous carbons in a cost-effective manner [1–3,11,21–24].

The conventional method for making MPRs entailed the usage of self-assembled network resins, such as phenol-formaldehyde (PF) resins oriented using block copolymer templates (such as P123 and F127). The orientation of phenol-formaldehyde moieties was incumbent on strong hydrogen bond

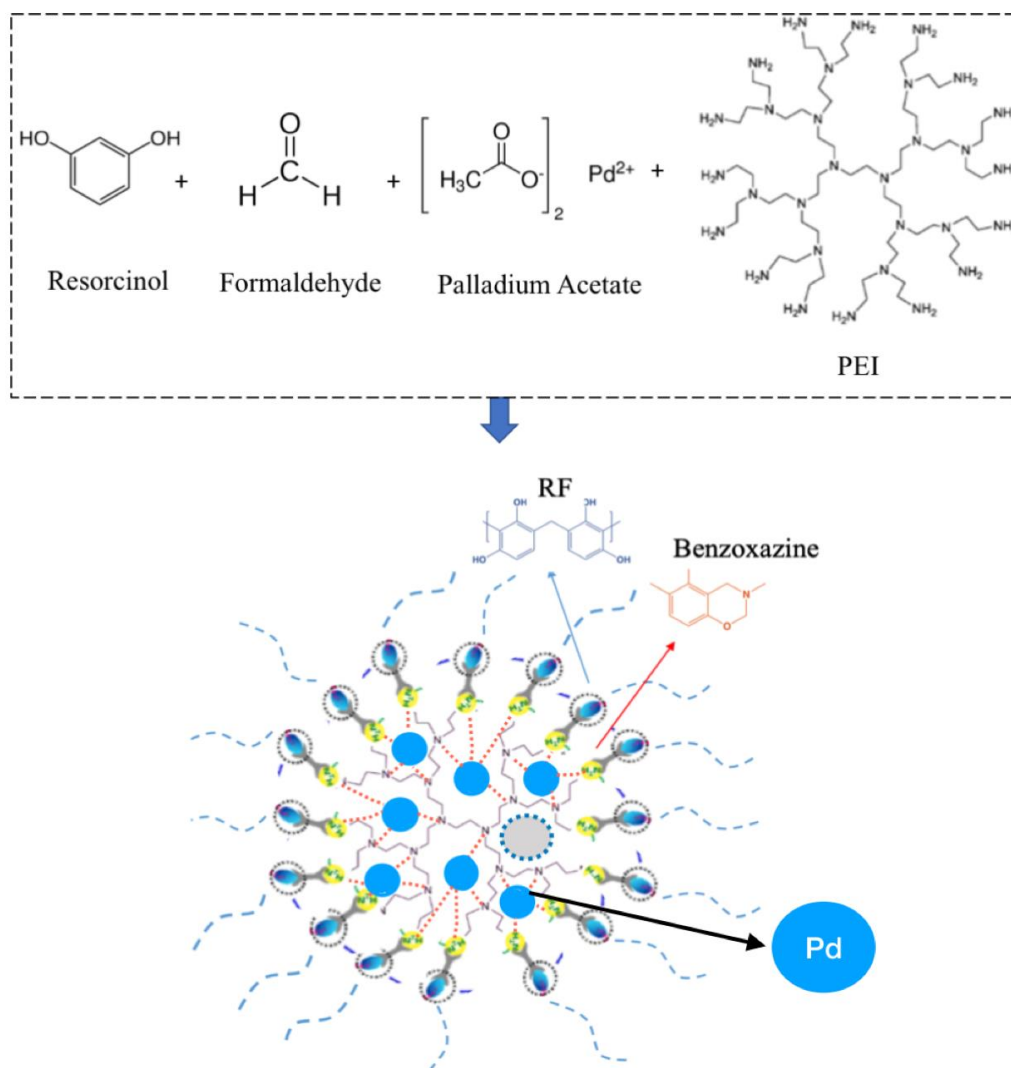
interaction with the pluronic template [1–4,11,24]. The mesoporous structure can be produced by two types of templates: (1) supramolecular aggregates such as surfactant micelle arrays (made from block copolymers) and (2) rigid mesoporous solids which are performed, such as mesoporous silica and colloidal crystals [7,8]. When supramolecular micellar aggregates are used, the process is called soft templating, while the method involving rigid mesoporous templates is known as hard templating or nanocasting. The template must be removed after the process of synthesizing the mesoporous polymer is over. The primary limitation of using a template is difficulties in its removal after pore construction. The process of template removal is complicated and adds unit operations and costs to the process of MPR synthesis.

In addition to the template, a central role is played by the interface in processing. The interface between the template material and the actual polymer (which will orient itself around the template to form the mesoporous solid) is crucial to the assembly and construction of the mesostructure. The interaction is considered to be critical in governing the soft template route for the synthesis of MPRs' materials. The method of using these external templates has significant limitations. The final products are obtained in the form of the powder which prevents their application as films and makes molding into specific shapes. There is also a limit to the sizes and patterns of mesopores obtained.

Also, conventional MPR synthesis requires the use of organic solvents with acid or base catalyst and curing at temperatures from 75 °C–260 °C to crosslink phenol-formaldehyde precursors. Although this high-temperature hydrothermal synthesis ensures complete cure and enhanced thermomechanical stability of the PF resin [4], it also entails concerns of safety with the use of solvents at high temperature, in additions to concerns for environmental safety. MPR networks, prepared as said-from the condensation of phenolics with aldehydes-result in catalytically inert networks. To incorporate catalytically active heteroatoms, the synthesis must either include the use of appropriate precursors or incorporate these heteroatoms post-treatment. However, these processes may partially destroy the mesoporous structure in the MPRs. This results in ill-dispersed active catalyst sites [22–26]. The primary reason is attributed to the lack of appropriate sol-gel methods for precursors. Additionally, their air and water sensitive features are considered a bane. This calls for the development of a synthetic organic solvent free as well as a template-free process for the preparation of MPRs. PEI is a polymer with amine-containing repeat units, spaced out by an aliphatic ethylene  $\text{CH}_2\text{CH}_2$  linkage. PEI can be synthesized as linear, highly dendrimeric, or branched polymers [27]. The hypothesis of the formation of a porous structure using PEI involves the crosslinking of the resorcinol-formaldehyde (RF) resin using a branched dendrimeric PEI that provides a large number of primary amines participating in the crosslinking (Scheme 1). The primary amines participate in the crosslinking mechanism and as a result orient the resorcinol-formaldehyde pre-polymer along the lines of its own dendrimeric structure. The dendrimeric structure hence controls the extent and the type of porosity obtained in the final mesoporous structure. In fact, The highly branched dendrimeric form of the PEI integrates into the chemical structure and provides porosity [27–30].

In the paper, we present a novel one-pot aqueous phase synthetic method for making a phenolic mesoporous resin containing well-dispersed Pd nanoparticles without the usage of a template and organic solvent. Elimination of a template reduces at least one or two unit operations entailing template breakdown and purification of the MPRs thus making this process conducive to scaling up. The elimination of an organic solvent also, significantly, establishes a green, low-toxicity process, laying the foundation for ease of scale-up, decrease the production cost and applicability. Also, the proposed synthesis method offers a novel approach for anchoring metal particles in the structure of the catalyst polymer network for the efficient cross-coupling reaction to produce fine chemicals. Pd containing MPRs (Pd-MPRs) were synthesized using polyethyleneimine (PEI) in either water or ethanol/water media and loaded with varying levels of Pd nanoparticles. Since hyperbranched PEIs are liquids at room temperature, the “body” of the resultant solid will be provided by the crosslinking and characteristics of the RF resin, while the involvement of the PEI will control the porosity. Thus, the polymerization of resorcinol and formaldehyde is accompanied by a reaction between amine groups

in the PEI and resorcinol and formaldehyde as well as pre-polymerized linear oligomers of RF leading to the formation of benzoxazine rings in the crosslinked and porous polymeric network. Since the process does not involve an external template and can be accomplished in a one-pot synthesis procedure, from a commercial processing point-of-view, major advantages include: (1) the reduced number of unit operations due to the absence of the template removal step, and (2) the ease of production and low manufacturing cost due to the elimination of wash solvents [31,32].



**Scheme 1.** Aqueous phase synthesis of Pd containing mesoporous polymeric resins, where RF represents the resorcinol-formaldehyde component of the formed crosslinked polymeric network.

Furthermore, the MPRs were observed to allow sufficient loading of Pd nanoparticles for effective catalytic activity due to unique interactions between the Pd ions and amino groups during material synthesis [15]. The structure-catalytic performance relationship of the developed Pd-MPRs was determined via batch Suzuki-Miyaura cross-coupling (SMC) reactions and continuous SMC reactions in a microreactor.

## 2. Results

### 2.1. Nitrogen Adsorption-Desorption Analysis

The Brunauer–Emmett–Teller (BET) surface area was calculated based on N<sub>2</sub> adsorption isotherms (Table 1). The table also includes Non Localized Density Functional Theory (NLDFT) data. Figure 1a shows that the PEI concentration plays a vital role in enhancing the surface area. The resin (RF) made without PEI shows a significantly lower surface area with no porous structure. The addition of 110 mg PEI (1.96 wt %) to the reaction mixture results in a nearly 590% increase in surface area over the resin made without PEI. The relationship is not linear, as a further doubling in the amount of PEI to the reaction mixture to 220 mg (3.93 wt %) reduces the surface area by nearly 35% compared to 110 mg of PEI. The addition of PEI influences RF resin development, resulting in the formation of pores. However, too much PEI may result in “liquid” blocking of the developed pores, resulting in surface area reduction, as seen with the 220 mg PEI MPRs. Any further addition of PEI beyond the limit of crosslinking, determined by the relative stoichiometric ratios of the components, may have merely caused the PEI to enter the pores as a “liquid” blocking the pores resulting in the aforementioned 35% reduction in surface area. A control MR with 0% PEI was also made, which had a very low (14 m<sup>2</sup>/g) BET surface area.

**Table 1.** Surface Area and volume distribution of various catalysts based on BJH and NLDFT models (RF = non-porous resorcinol-formaldehyde resin, 110 and 220 = 110 mg and 220 mg PEI respectively; EW = ethanol-water, W = water solvent P1 and P3 = 1 wt % Pd and 3 wt % Pd, respectively).

|              | Surface Area (m <sup>2</sup> /g) |             |     |       | Pore Volume (cc/g) |       |
|--------------|----------------------------------|-------------|-----|-------|--------------------|-------|
|              | BET (Meso)                       | BET (Micro) | BJH | NLDFT | BJH                | NLDFT |
| RF           | 14                               | 20          | 8   | 13    | 0.033              | 0.030 |
| MPR110-EW    | 207                              | 326         | 315 | 390   | 0.350              | 1.522 |
| MPR220-EW    | 80                               | 212         | 80  | 167   | 0.340              | 0.274 |
| MPR110-EW-P1 | 108                              | 257         | 109 | 177   | 0.240              | 0.175 |
| MPR110-W-P1  | 74                               | 149         | 74  | 114   | 0.850              | 0.493 |
| MPR110-W-P3  | 129                              | 205         | 129 | 139   | 0.170              | 0.802 |
| MPR110-EW-P3 | 226                              | 432         | 226 | 384   | 0.350              | 0.447 |
| MPR220-EW-P3 | 123                              | 342         | 123 | 236   | 0.140              | 0.241 |

We also evaluated the effect of palladium concentration on the surface area of the Pd-MPRs (Figure 1b). The surface areas of MPR110-EW, MPR110-EW-P1 and MPR110-EW-P3 are 326, 257, and 433 m<sup>2</sup>/g, respectively (110 and 220 stand for 110 mg and 220 mg PEI, respectively; EW stands for ethanol-water solution, W stands for water solution; P1 and P3 stand for 1 (wt %) Pd and 3 (wt %) Pd, respectively). As seen in Figure 1b, the increase in Pd acetate content from 0 (wt %) to 3 (wt %) results in a significant increase in the surface area of MPRs containing the same concentration of PEI. The increase in surface area can be attributed to the formation of organometallic complexes between Pd and the nitrogen of the PEI, which tends to anchor and orient the PEI dendrimers as well as the RF moieties in spatially aligned networks contributing to enhanced porosity in general.

Figure 1c explores the effect of water versus ethanol/water as the solvent medium in the Pd-MPRs synthesis. While in ethanol/water as a reaction medium, the addition of 3 wt % Pd acetate causes an increase in the surface area (as also seen in Figure 1a), the use of water as the reaction medium causes a slight decrease in the surface area in a comparable reaction set up. The explanation could be tied to the solubility of the Pd acetate. Pd acetate is soluble in organic solvents. However, it has low solubility in water. As a result, in a poor distribution of Pd centers, incapable of orienting the nitrogen atoms of the PEI and RF moieties, through coordinate bonding, or clustering of Pd acetate, in the porous structure.

Consequently, it leads to a lower surface area when compared to that obtained using ethanol as the solvent. Despite this, making the porous catalyst in the water phase makes the catalyst synthesis more environmentally friendly, with less of a downstream process to reuse the solvent phase.

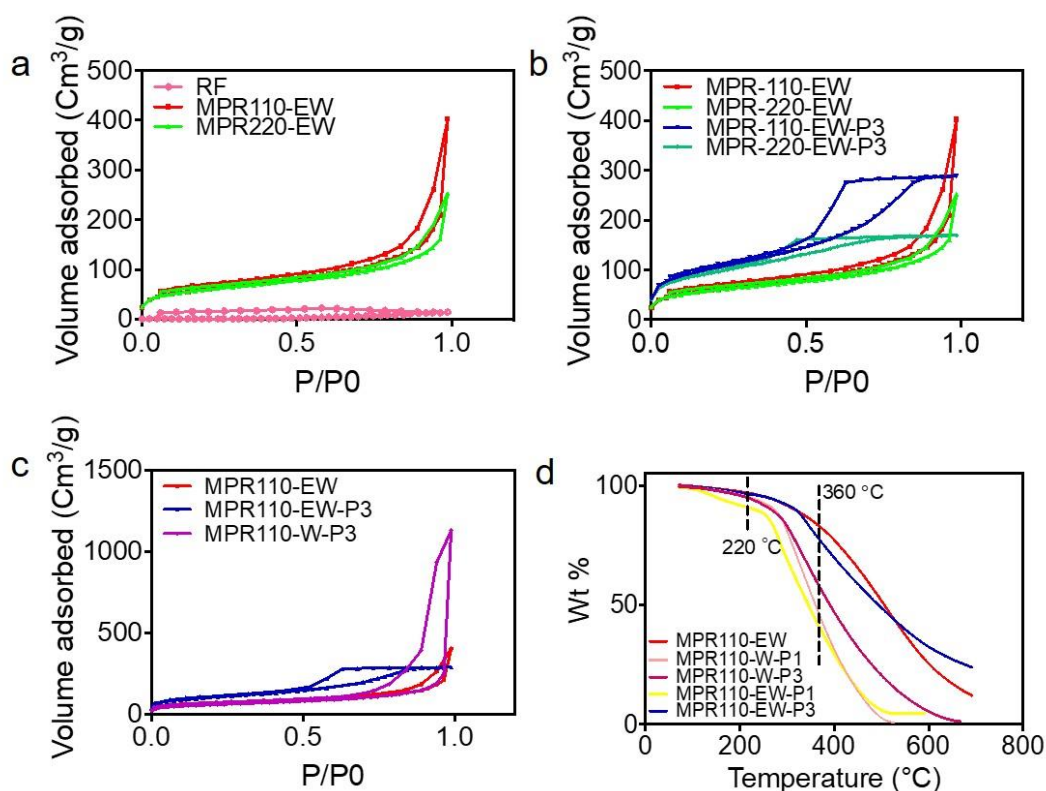


**Figure 1.** (a–c) N<sub>2</sub> adsorption–desorption isotherms of (a) MPR with varying PEI concentration, (b) Pd-MPRs with varying Pd concentrations, and (c) Pd-MPRs made either in the presence of water or water/ethanol as the solvent. (d) Thermal stability of MPR with varying PEI concentration (RF = nonporous resorcinol-formaldehyde resin; 110 and 220 = 110 mg and 220 mg PEI, respectively; EW = ethanol-water; W = water solvent; P1 and P3 = 1 wt % Pd and 3 wt % Pd, respectively).

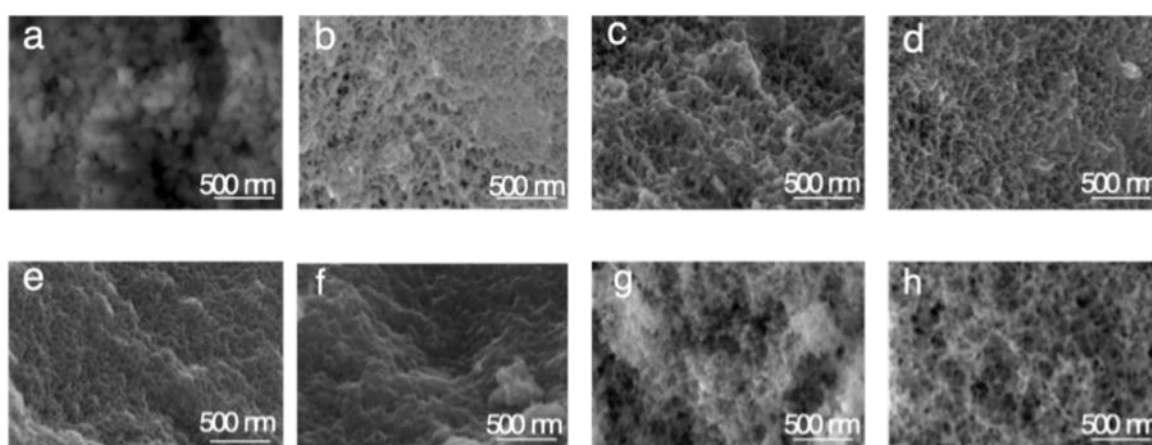
## 2.2. Thermogravimetric Analysis (TGA)

Figure 1d illustrates the comparative thermal stabilities of the synthesized MPRs. In general, the MPR showed high thermal stability up to the temperatures of 320 to 360 °C. The addition of 1 (wt %) Pd causes a steeper weight loss starting at around 220 °C versus the weight loss commencement. With an increase in the Pd loading to 3%, the sharpness of the weight loss is also less. The weight loss seems the least sharp with the usage of 3% Pd. From Figure 1d it can be inferred that the mesoporous resin held onto a significant amount of water, due to the usage of PEI, which induced hydrophilicity due to the presence of amine groups. The heating kick-starts water evaporation and hence the apparent weight loss at an earlier temperature. The reaction mixture in ethanol may have lost its solvent from its porous interstices due to the lower affinity of ethanol for the amino groups in PEI as well as ethanol's higher intrinsic volatility.

## 2.3. Scanning Electron Microscopy (SEM)

Figure 2a–h shows the SEM images of the mesoporous catalyst with various compositions. Compositions made with palladium acetate and an ethanolic solution of PEI are seen to exhibit a uniform morphology with an interconnected framework and visible uniform micropores. These SEM images confirm the average pore size of the various catalyst and they are listed in Table 1. The morphology of the resin compositions made without PEI is found to be spherical (Figure 2a).

The addition of ethanolic PEI solutions was observed to increase pore interconnectivity. With the immobilization of Pd to these compositions, a further increase in pore interconnection was observed with a concomitant increase in the surface area as mentioned above. The same compositions, with immobilized Pd, however, using water instead of ethanol as the medium for synthesis, showed a non-uniform pore interconnection. These changes may be correlated with the results obtained with the BET isotherms in Figure 1, attributed to the formation of coordination complexes between Pd and the donor nitrogen atoms of PEI and the RF (including the benzocaine ring) anchoring and orienting the dendrimers to result in the structured interconnected porous network design rendered by the spatial alignment of polymer networks. Again, the poor solubility of Pd acetate in water and concomitant phase separation, renders Pd atoms incapable of uniform coordination with N atoms of PEI and benzoxazine groups, resulting in a poor spreading and inferior spatially connected network formation. Also, a competition between the oxygens of water and N atoms of the PEI for anchoring the Pd atoms may result in the randomness of the network shape.



**Figure 2.** SEM of various samples: (a) RF (b) MPR110-EW, (c) MPR220-EW (d) MPR110-EW-P1 (e) MPR110-EW-P3 (f) MPR110-W-P1 (g) MPR110-W-P3 and (h) MPR220-EW-P3. (500 nm).

#### 2.4. TEM and XPS and Elemental Analysis

The transmission electron microscopy (TEM) image of MPR110-EW-P1, supported the existence of uniform mesopores inside the network (Figure 3a,b). The black spots may be concluded as Pd(0). The existence of Pd is corroborated with the XPS spectra of the compositions. Figure 4a–c shows the XPS spectra of MPR110-EW-P3, which show peaks associated with C 1s, N 1s, and Pd 3d. The deconvolution and fitting of the C 1s spectra yielded three peaks at around 284.8 and 286.2 eV and 288. These were attributed to C–C bonds of the aromatic benzene ring, C–N and O–C=O bonds. The N1s peaks at around 387 and 405.5 eV belonged to amino group nitrogen and those associated with Pd through coordination. The peaks of Pd 3d at ~336.56 and 341.8 eV were those of Pd<sup>0</sup>. The peaks at ~338.6 and 343.2 eV were assigned to Pd<sup>2+</sup>. Pd was hence concluded to have been incorporated successfully within the MPR compositions in various valence states. The coordination bonding with the Ns of the various amino groups and the nitrogen of the benzoxazine groups in the sample could be the reason for strong bonding. Figure 5a,b and Table 2 present the EDX elemental analysis for MPR110-EW-P3 catalyst. The results confirm a relatively high amount of nitrogen atoms (7–11% *w/w*) in the catalyst structure which is related to the amine groups in the PEI structure. The high content of nitrogen atoms is a good indication for strong interaction of Pd and amine group in the sample as observed in XPS data.

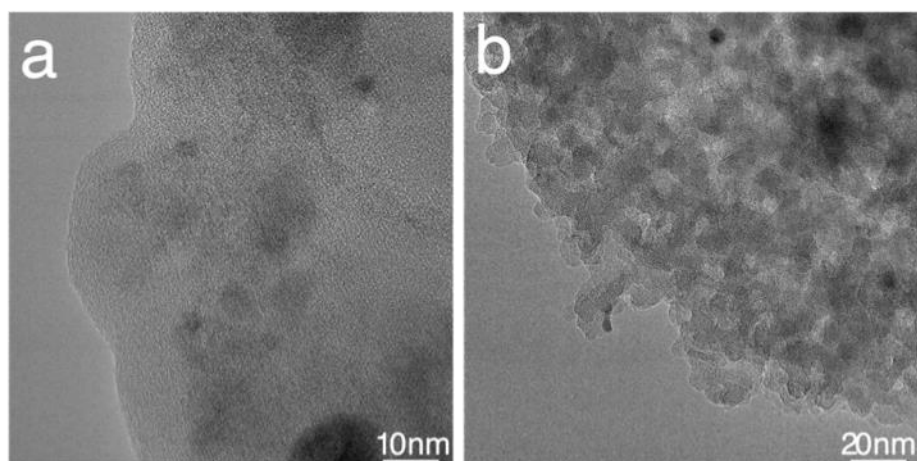


Figure 3. TEM image of MPR110-EW-P3 with (a) 10 nm and (b) 20 nm scale bar.

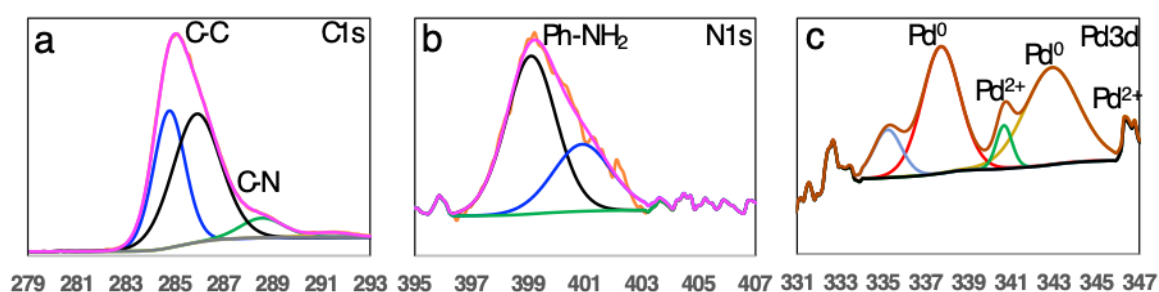


Figure 4. XPS spectra of (a) C 1s, (b) N 1s and (c) P 3d of MPR110-EW-P3.

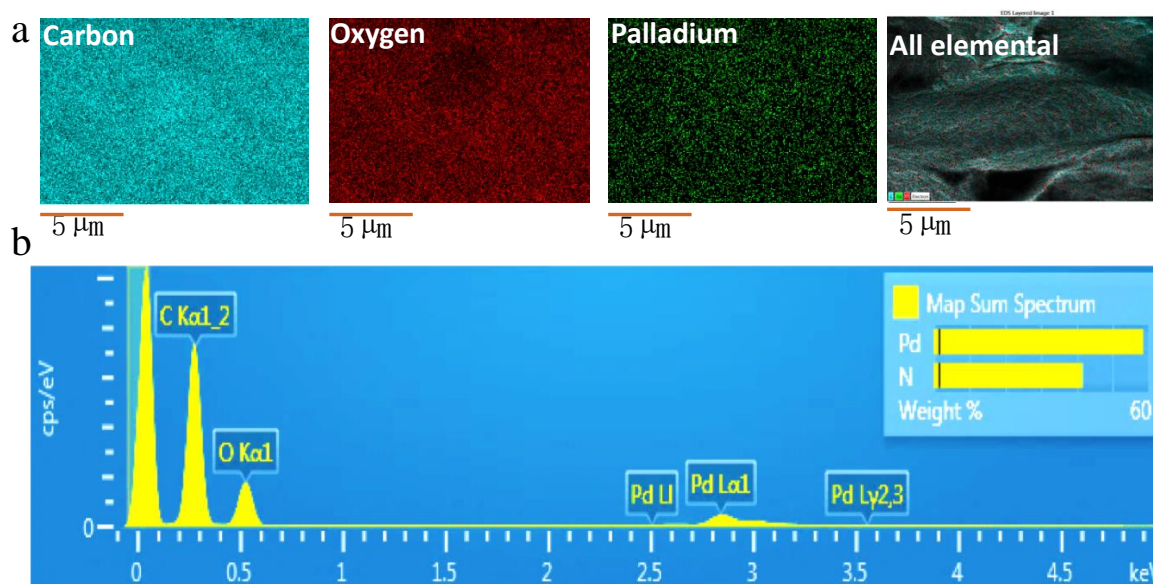


Figure 5. SEM-EDS elemental mapping of MPR110-EW-P3 where (a) analogous elemental mapping of the element Carbon, Oxygen, Palladium and all, scale bar 5  $\mu\text{m}$  (b) Area EDS spectrum for Table 2 for the atomic and weight percentage of various elements

**Table 2.** Carbon, Oxygen, Nitrogen and Palladium in various Pd-MRs catalyst based on EDS.

| Sample      | Carbon | Oxygen | Nitrogen | Palladium |
|-------------|--------|--------|----------|-----------|
| MR110-EW    | 50.14  | 41.55  | 8.31     | 0         |
| MR110-EW-P1 | 53.32  | 37.62  | 7.25     | 1.55      |
| MR110-W-P1  | 51.87  | 35.42  | 11.08    | 1.63      |
| MR110-W-P3  | 52.67  | 10.34  | 36.75    | 0.25      |
| MR110-EW-P3 | 55.58  | 36.96  | 7.31     | 0.16      |
| MR220-EW-P3 | 54.67  | 37.12  | 7.42     | 0.79      |

### 2.5. Catalytic Application

The catalytic efficiencies of the mesoporous catalysts, made with various compositions and under different reaction conditions, were tested in typical Suzuki-Miyaura reaction batches. The C-C bond of 4-iodotoluene was reacted with aryl boronic acid under mild conditions comprising the ethanol-water reaction medium and potassium carbonate as the base. Figure 6a,d shows the schematic of Suzuki-Miyaura reactions in a batch system using Pd-MPRs as catalysts for iodotoluene (using ethanol as solvent) and bromotoluene (using dimethylformamide (DMF) as solvent), respectively. The conversion versus time is shown for the respective reactions in Figure 6b,e. The conversion climbs up faster and more abruptly, reaching a higher final value for the iodotoluene reaction. The primary difference between the two reactions could be attributed on one hand to the intrinsically more “labile” carbon-iodine bond in the iodotoluene, and on the other hand to the presence of different solvent systems in the two cases. The DMF solvent system is also expected to cause some amount of catalyst poisoning which reduces the rate of the reaction as well as the overall conversion. The catalyst MPR110-EW-P3 with the highest surface area (433 m<sup>2</sup>/g) showed the maximum conversion rate of 98.98%. A control MR with 0% PEI was made and tested. In addition to a very low (0–2 m<sup>2</sup>/g) BET surface area, we obtained only 6.8% conversion.

In general, the results showed the catalytic efficiency of the Pd-MPRs depends on the type of PEI solution used to make the mesoporous catalyst and the percentage of palladium immobilization in the catalyst structure. The catalysts made using PEI in ethanol/water, and those with a higher amount of Pd immobilization have superior catalytic activity. The amount of active Pd sites is directly related to the center of coordinated catalytic sites available for the reaction. The usage of water rather than ethanol/water in mesoporous catalyst synthesis has a direct bearing on the surface area and the porosity obtained with the catalyst, which in turn, affects the diffusivity of reactants onto the active sites and hence the ensuing results. Additionally, we surmise that the lower solubility of Pd salts in water may have led to a non-uniform distribution of Pd anchoring centers in the catalyst structure. This would lead to clustering and poor extent of coordination with the PEI dendrimers and benzoxazine groups which automatically decreases the easy and uniform availability of active catalytic centers, hence corroborating the results.

The same Suzuki-Miyaura coupling of the C–C bond of 4-bromotoluene (Figure 6d–f) with aryl boronic acid in the presence of DMF water and potassium carbonate at 110 °C was also undertaken.

The reaction conversion rate for various catalysts is shown in Figure 6e. The results show that MPR110-EW-P3 has a maximum conversion rate of 88.5% after 5 h. After 5 h, the conversion rate stagnates due to the saturation of the catalyst surface by the aromatic compound. The conversion rates of MPR110-EW-P1, MPR110-W-P3, and MPR110-W-P1 are 77%, 55.2%, and 65% respectively after 5 h underscoring that while an increase in Pd content enhances the catalytic capacity, the effect that water has on clogging pores and reducing surface area is more detrimental to make up for the increase in catalytic activity. These results showed that surface area and the solvent used to dissolve PEI for making the catalyst played essential roles in catalyst efficiency.

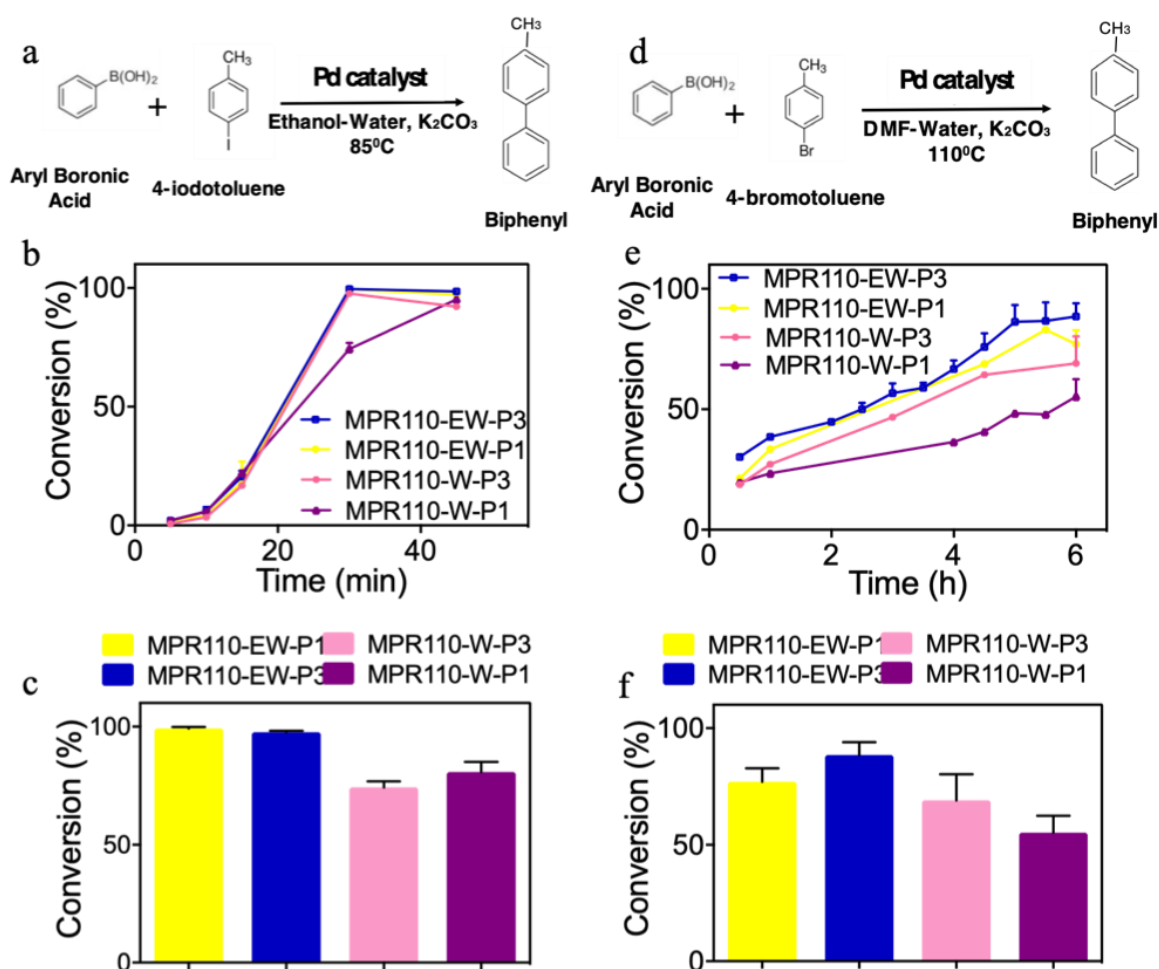


**Figure 6.** Suzuki-Miyaura reaction in the batch system (a) Reaction schematic for Iodotoluene, (b) Conversion rate: Conversion % vs. time for Iodotoluene and ethanol as solvent, (c) Effect of catalyst type on conversion rate for Iodotoluene and aryl boronic acid in the present of ethanol as solvent, (d) Reaction schematic for Bromotoluene, (e) Conversion rate: Conversion % vs. time for Bromotoluene and DMF as solvent (f) Effect of catalyst type on conversion rate for Boromotoluene and aryl boronic acid in the present of DMF as solvent ( $n = 3$ ).

We studied the recyclability of MPR110-EW-P3 in the model SMC reaction. Figure 7a shows the Suzuki-Miyaura reaction conversion rate in a batch system for iodotoluene after 5 cycles ( $n = 3$ ). Figure 7b shows the SEM and the corresponding EDX elemental mapping analysis for used MPR110-EW-P3 after 5 runs. After each reaction cycle, the catalyst was separated by filtration and then washed thoroughly with copious amounts of cold water-ethanol solution, and the recovered catalyst was dried under vacuum at 40 °C for 2 h. Thus, purified, the catalyst was re-employed in five successive cycles under equivalent conditions. As shown in Figure 7b, the percentage of conversion rate was almost the same for all these runs (up to 98.9%).

Recyclability of MPR110-EW-P3 in Suzuki-Miyaura reaction conversion rate for bromotoluene in DMF as a solvent for 3 cycles ( $n = 3$ ) is shown in Figure 7c. After each run, the catalyst was separated by filtration and then washed with copious amounts of cold DMF followed by water. The catalyst was dried under vacuum at 40 °C overnight and then reused for the next run. The activity reduced from  $86.3 \pm 3\%$  in the first run to  $80.5 \pm 2\%$  and  $80.3 \pm 4\%$  in the second and third run, respectively. Based on the above results, and as per previous literature reports, catalyst activity decreases because of leaching palladium and shrinkage of the structure. Surface area declined for this catalyst in DMF solution more than five times. The DMF water medium for the second group of SMC reactions has a detrimental

effect with progressive runs on the breakdown of the structure of the catalyst as well as rapid clogging of pores resulting in the reduction of surface area with the ensuing decrease in catalytic efficiency.

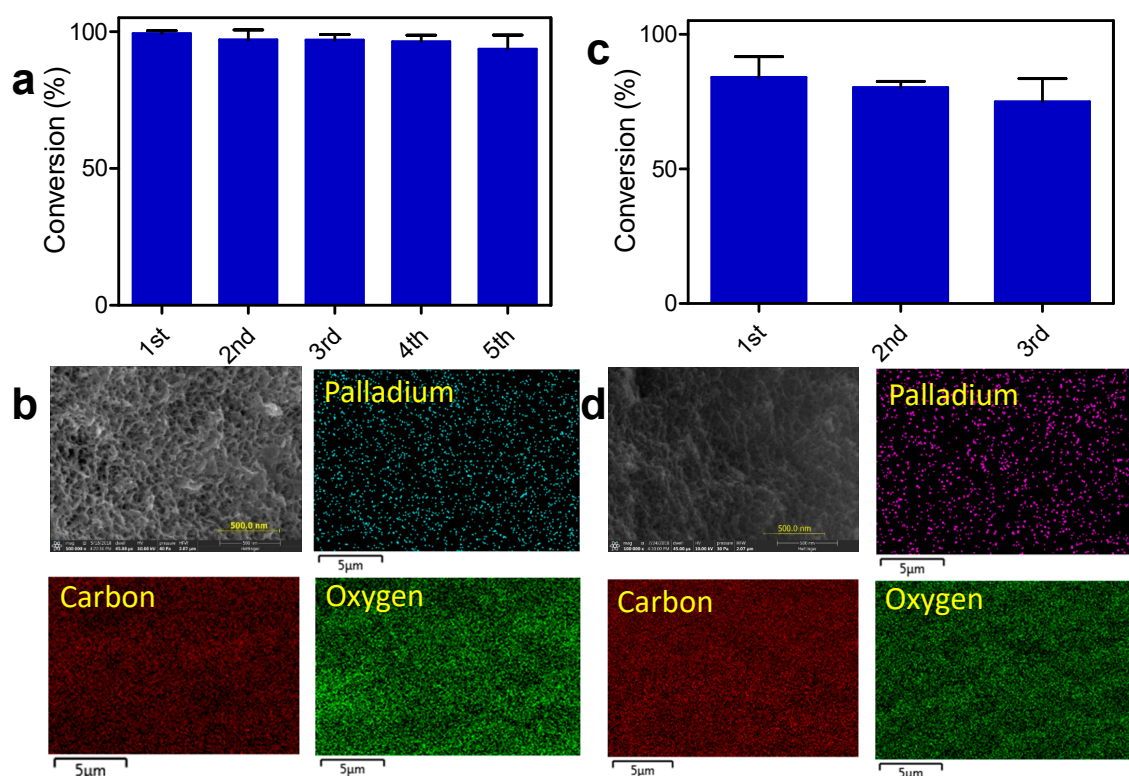


**Figure 7.** (a) Suzuki-Miyaura reaction conversion rate in batch system for Iodotoluene with ethanol as solvent for 5 reaction cycles ( $n = 3$ ), (b) SEM, and the corresponding EDS elemental mapping analysis for used MPR110-EW-P3 3% after 5 runs in ethanol-water as solvent (c) Suzuki-Miyaura reaction conversion rate in batch system for Bromotoluene and DMF as solvent for 3 cycles ( $n = 3$ ), (d) SEM, and the corresponding EDS elemental mapping analysis for used MPR110-EW-P3 after 3 cycles with DMF—water solvent.

## 2.6. Continuous Suzuki-Miyaura Reaction in a Microreactor

To establish the efficiency of the heterogeneous Pd-MPRs catalyst in a continuous flow set up, a fixed bed microreactor was employed. A schematic of the microreactor set up and results of the continuous reaction are shown in Figure 8a. C–C bond coupling between 4-iodotoluene and aryl boronic acid, as the SMC reaction model. The U shape micro tube provides enough length of catalyst for proper residence time, as shown in Figure 8. Various process parameters, such as the inlet flow rate and temperature, were considered and varied for studying the system. The conversion rate during the reaction time confirmed that the continuous process is the almost steady state and catalyst efficiency remains at a steady and stable value for up to 20 min for minimum and maximum flow rate (0.1 and 0.5  $\mu\text{L}/\text{min}$ ) (Figure 8b). Additionally, Figure 8c shows the effect of temperature on the conversion rate for 4-Iodotoluene and ethanol as solvent at an initial velocity of 0.1  $\mu\text{L}/\text{min}$ . Figure 8d shows the effect of velocity on the conversion rate for 4-Iodotoluene and ethanol as a solvent at 85  $^{\circ}\text{C}$ . On increasing the temperature from 65 to 86  $^{\circ}\text{C}$ , the conversion rate was enhanced from 51.6 to 60.7% at the initial flow rate of 0.5 ( $\mu\text{L}/\text{min}$ ). Increasing the flow rate can increase the conversion rate by enhancing the mass transport coefficient. On the contrary, however, this resulted in decreased residence time inside the reactor [28]. Therefore, it is not possible to observe a linear relationship between flow rate and conversion. The maximum conversion rate was reported for 0.2  $\mu\text{L}/\text{s}$  (61.6%), and after that it decreased to 46.4% at a flow rate of 0.4  $\mu\text{L}/\text{s}$ . This translates to a space velocity of 0.1 and 0.5  $\text{h}^{-1}$ , respectively.

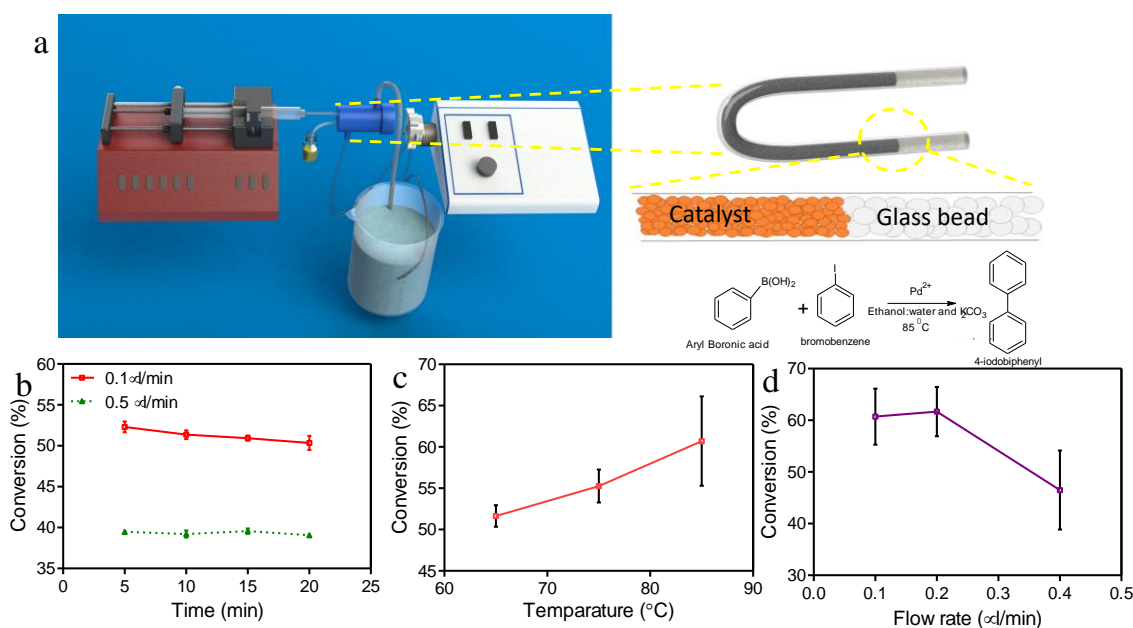


**Figure 8.** Suzuki-Miyaura reaction in the microreactor. (a) Microreactor set up (b) Velocity effect on conversion rate for 4-Iodo toluene and ethanol as solvent at 65 °C during time (c) Temperature effect on conversion rate for 4-Iodo toluene and ethanol as solvent at initial velocity of 0.1 μL/min (d) Velocity effect on conversion rate for 4-Iodo toluene and ethanol as solvent at 85 °C (n = 3).

### 3. Discussion

While mesoporous molecular silica or alumina sieves have been widely studied for anchoring Pd species, their hydrothermal instability limits high-temperature catalytic applications [33,34]. Thus, anchoring of Pd to the mesoporous catalyst structure was attempted, by employing alternate functional groups, such as metal-organic frameworks [35], magnetic supports [36], carbons [37], and polymers [38,39]. The use of a functional framework, one end of which is tethered to the main mesoporous catalyst structure while the other end is likely managing to hold the Pd (II) moiety. This is expected to provide for a superior and a more uniform distribution of active metal centers. The only limitation that may occur with this method is the control of reactivity by the anchoring functional group, which may reduce the catalytic activity of the Pd center towards the intended reaction [34]. The amine group was widely studied by way of (3-aminopropyl) triethoxysilane (APTES) [40,41], which is a good electron donor (NHC donor) and Pd anchoring group for coupling catalysis. N-heterocyclic groups have also been similarly used to anchor Pd with the concomitant formation of NHC donor-Pd catalysts for coupling reactions [42,43]. In this light, we may be able to visualize the anchoring of Pd in our work as schematically shown in Scheme 1 [34]. The Pd may be expected to be dispersed and held in place by the tertiary nitrogens from the PEI branched structure, as well as, to a lesser extent, from the N in the benzoxazine ring, due to the -I effect of the oxygen atom to the N in the benzoxazine.

Scheme 1 depicts the positions and anchoring of Pd centers in the PEI-RF network. As mentioned earlier, the lone pair of electrons on the tertiary nitrogen of the PEI as well as those in the benzoxazine group engage with the Pd (II) center, and one nitrogen atom may coordinate once with a Pd center given the presence of only one lone pair of electrons per N atom. Pd (II) is known to form mostly four coordinated square planar complexes. Thus, the Pd is expected to anchor and form a complex where the structure of the RF-PEI infinite network provides four N centers in a square planar formation. In the absence of sufficient donor groups surrounding the Pd center in a square planar formation, not every “cavity” formation offered by the mesoporous network may successfully anchor and hold onto a Pd center, even if stoichiometric equivalence may allow so, and this is depicted in Scheme 1 depicting an empty “cavity”. Pd (II) has an electronic configuration of containing 8 electrons in the 4d

orbitals. The remnant available  $dz^2$  may hybridize with the 5s and two 5p orbitals to form four  $dsp^2$  hybridized orbitals oriented in a plane for accepting electron donors, such as the lone pair of the p orbitals of the N atoms. Thus, the anchoring of Pd (II) species may be limited by the presence of four neighboring N atoms in a square planar formation. From Scheme 1 there may be a paucity of N donors towards the periphery of the “globe” shown and the coordinating N atoms predominantly arise from the benzoxazine group. However, the PEI-RF network is an “infinite” three-dimensional network and only a visualizable symmetric section is shown in Scheme 1. Thus, the origin of the N donor atom-PEI vs. benzoxazine is dependent on the relative stoichiometry of PEI: RF used in the reaction.

The cross-coupling in the Suzuki-Miyaura Pd catalyzed coupling goes through oxidative addition, followed by transmetallation and reductive elimination [34]. The rate constant of Suzuki couplings is known to be dependent on the Pd-donor ligand binding energy [44]. There may be a subtle difference in the donor ability of the nitrogen centers in the PEI versus that in the benzoxazine. Both the nitrogens are in the proximity of electron withdrawing electronegative atoms. In the benzoxazine group, the N is separated from oxygen by one  $CH_2$  link, while in PEI, the N is separated from another N by a  $CH_2-CH_2$  link. The benzoxazine N, due to closer proximity to a more powerful electron withdrawing entity (oxygen), is expected to render itself as a weaker donor to the hybridized  $dsp^2$  orbitals of Pd (II), making it more available as a base for the coupling. However, there may be an offset on the benzoxazine nitrogen’s fundamental ability as a Lewis base due to its intrinsic proximity to oxygen trying to polarize the electron cloud towards the latter via a secondary -I effect. The stoichiometric ratio of benzoxazine nitrogen and PEI nitrogen may provide for an interesting future study on the kinetics of Suzuki couplings.

Additionally, the activity studies on immobilized Pd catalysts versus that in the form of homogenous complexes underscore the fact that Pd (II) acts as a catalyst in the heterogeneous rather than the homogenous form [45]. Thus, the development of a scalable, easy to manufacture catalyst structure, which may be retrofitted in versatile manners from the industrial plug flow bed type reactor designs to simple micro designs for biomedical applications, underscores the importance of this catalyst design method for Suzuki-Miyaura couplings under mild conditions with versatile reactions for wide application vistas.

## 4. Materials and Methods

### 4.1. Materials

Resorcinol, 98%, formaldehyde 37%, palladium acetate and PEI 99% (molecular weight 10,000 DA) were purchased from Alfa-Aesar (Ward Hill, MA, USA) and used without purification.

### 4.2. Synthetic Procedures

MPRs and Pd-MPRs were synthesized in one-step by the reaction between resorcinol, formaldehyde and PEI in water or ethanol solution. As a typical run, 1.5 g resorcinol was dissolved in 4.4 mL of distilled water with vigorous stirring in a water bath (40 °C) to obtain a clear solution. Then, 5.6 mL of 1.96 or 3.93 w/v% aqueous or ethanolic PEI solution was added to it and kept in the water bath for 15 min. Sequentially, palladium acetate powder was added and kept stirring for 20 min. Finally, 2.1 mL of formaldehyde (37% in water) was injected at a high stirring speed (up to 750 rpm). After 20 min, the solution was poured in a Teflon hydrothermal autoclave chamber and baked for 12 h at 120 °C. The synthesized Pd-MPRs were washed with deionized water (DI) water and dried under vacuum at room temperature. The catalyst was ground and sieved for reaction efficiency consideration. A control MR was also made with 0% PEI.

### 4.3. Characterizations

The N<sub>2</sub> adsorption and desorption analyses were measured using a NOVA Touch LX4 Surface Area Analyzer (Quantachrome, Boynton Beach, FL, USA) to determine the surface areas and volume

distributions of the synthesized materials. X-ray photoelectron spectra (XPS) characterizations were performed on a PHI model Quantum 2000 spectrometer with scanning ESCA multiprobe (Physical Electronics Industries Inc., Chanhassen, MN, USA) and with using Al K $\alpha$  radiation ( $I = 1486.6$  eV) as the radiation source. The spectra were recorded in the fixed analyzer transmission mode with pass energies of 187.85 eV and 29.35 eV for recording survey and high-resolution spectra, respectively. The powder samples were pressed on a double-sided carbon tape mounted on an Al coupon pinned to a sample stage with a washer and screw then placed in the analysis chamber. Binding energies (BE) were measured for Pd 3d, N 1s, C 1s and O 1s. The XPS spectra obtained were analyzed and fitted using CasaXPS software, version 2.3.16, (CASA Software Ltd., Bidford, UK). Sample charging effects were eliminated by correcting the observed spectra with the C 1s BE value of 284.8 eV. The thermogravimetric properties of the synthesized materials were measured using a TA Instruments Q500 thermogravimetric analyzer (New Castle, DE, USA). Approximately 5 mg of sample was placed in a platinum pan and heated to 700 °C at a rate of 10 °C/min in a N<sub>2</sub> atmosphere (40 mL/min balance gas flow rate and 60 mL/min sample gas flow rate). Thermo Scientific™ Quanta™ line 650 scanning electron microscopes (SEM) (Waltham, MA, USA) with a low vacuum detector, EDAX Electron Backscattering Diffraction, and Energy-Dispersive Spectroscopy were used for elemental mapping analysis and SEM. Aztec software (Oxford Instruments, Abingdon, UK) were applied to the analysis of EDAX data. JEOL 2010 FasTEM (JEOL USA Inc., Peabody, MA, USA) with an ultra-high-resolution pole-piece, was used for evaluating mesoporosity. The resolution is 0.14 nm. It is equipped with a Gatan Imaging Filter (GIF 2000) (Gatan Inc. USA, Pleasanton, CA, USA).

#### 4.4. Catalytic Activity

A 15 mL three-neck flask that was fitted with a reflux condenser was chosen as the reactor in all batch experiments. For Suzuki-Miyaura cross-coupling reactions, the flask was filled with a mixture of 0.25 mmol of 4-iodotoluene, 0.375 mmol of phenylboronic acid, 0.5 mmol of potassium carbonate, and 3 mL of ethanol and 1 mL water as solvents. This was followed by the addition of the catalyst (0.15 g) and the mixture was stirred at 80 °C for 45 min. Similarly, a mixture of 1 mmol 4-bromotoluene, 3.0 mmol of phenylboronic acid, and 2.0 mmol of potassium carbonate were added together and then 3 mL of dimethylformamide (DMF) and 1 mL of water were used as solvents. This reaction was performed for 5 h at 110 °C. The microreactor that was used for continuous reactor evaluations, was a U shaped plastic tube (0.22 mm OD and 0.2 ID) The tube was surrounded by a shell, fabricated using a Formlabs Form 2 SLA printer with their black resin (RS-F2-GPBK-04), with both the input and output of the temperature regulating fluid on the same side. The reaction temperature was adjusted and controlled by pumping hot water through the shell. A Harvard syringe pump was used to feed the reactor. For all experiments, the samples were analyzed with a Varian GC 3900 gas chromatograph (Agilent Technologies, Santa Clara, CA, USA), using a Factor Four VF-5ht capillary column (30 m  $\times$  0.25 mm ID), provided by Agilent Technologies (California, LA, USA), and raising the temperature from 50 to 200 °C at 20 °C min<sup>-1</sup>.

## 5. Conclusions

In this work, PEI, a dendrimeric polymer, was used to develop a novel template-free, simple, one-pot process for making a MPR structure. The mesoporous, template-free resorcinol-formaldehyde resin was used to immobilize palladium acetate, with resultant high surface area and interconnected porosity and distribution of Pd species guided by coordination complexes with the N centers. The Pd-MPRs catalyst exhibits excellent catalytic activity, applicability, and durability for the SMC reaction under varying conditions: mild and harsh with ethanol/water and DMF/water mediums, respectively. The Pd-MPRs catalyst can efficiently catalyze SMC reactions with conversions reaching between 95–98% within 45 min to 5 h, depending upon the exact conditions. The large surface area of the catalyst and high uniform distribution of Pd lead to excellent catalytic performance. The catalyst also shows excellent recyclability with minimal reduction in final conversions with repeated cycles.

Furthermore, high thermal stability and low Pd leaching underscore the potential of this catalyst as an excellent candidate for drug synthesis applications. Further investigations into the stoichiometric ratio of catalyst components, their effect on the catalytic structure and thereof on the SMC and catalytic mechanism would provide an interesting scientific platform for future study on the kinetics of Suzuki couplings. The catalysts were also tried in a micro-continuous PFR set up, under various process and flow conditions, realizing nearly a 62% conversion. This general protocol platform may open new opportunities for the development of the catalyst for wide application vistas, in particular for pharmaceuticals and therapeutics.

**Author Contributions:** Conceptualization, M.N., B.K., and I.N.; methodology, M.N., A.H., P.W., A.S.A., P.K., and I.N.; validation, I.N. and B.K.; formal analysis, M.N.; investigation, I.N.; writing—original draft preparation, M.N.; writing—review and editing, B.K. and I.N., S.S., J.F.S.III, F.L.; visualization, M.N., B.K.; supervision, I.N.; project administration, I.N.; funding acquisition, I.N., please turn to the CRediT taxonomy for the term explanation.

**Funding:** S.L.S is grateful for funding from the US Department of Energy, Office of Basic Energy Sciences, Division of Chemical, Biological and Geological Sciences under Grant DE-FG02-86ER13622.A000. We thank RIGAKU (USA) for XPS experiments.

**Acknowledgments:** The TEM studies were performed using the facilities at the University of Connecticut/Thermo Fisher Scientific Center for Advanced Microscopy and Materials Analysis (CAMMA). We also appreciate Stanzione's group to provide us facility for TG test at South Jersey Technology Park.

**Conflicts of Interest:** There are no conflicts to declare.

## References

1. Kung, S.C.; Chang, C.C.; Fan, W.; Snyder, M.A. Template-free ordered mesoporous silicas by binary nanoparticle assembly. *Langmuir* **2014**, *30*, 11802–11811. [[CrossRef](#)] [[PubMed](#)]
2. Muylaert, I.; Verberckmoes, A.; De Decker, J.; Van Der Voort, P. Ordered mesoporous phenolic resins: Highly versatile and ultra-stable support materials. *Adv. Colloid Interface Sci.* **2012**, *175*, 39–51. [[CrossRef](#)] [[PubMed](#)]
3. Martin, R.; Buchwald, S.L. palladium-catalyzed suzuki–miyaura cross-coupling reactions employing dialkylbiaryl phosphine ligands. *Acc. Chem. Res.* **2008**, *41*, 1461–1473. [[CrossRef](#)] [[PubMed](#)]
4. Wolfe, J.P.; Singer, R.A.; Yang, B.H.; Buchwald, S.L. Highly active palladium catalysts for suzuki coupling reactions. *J. Am. Chem. Soc.* **1999**, *121*, 9550–9561. [[CrossRef](#)]
5. Choma, J.; Jedynak, K.; Fahrenholz, W.; Ludwinowicz, J.; Jaroniec, M. Microporosity development in phenolic resin-based mesoporous carbons for enhancing CO<sub>2</sub> adsorption at ambient conditions. *Appl. Surf. Sci.* **2014**, *289*, 592–600. [[CrossRef](#)]
6. Liu, F.; Wu, Q.; Liu, C.; Qi, C.; Huang, K.; Zheng, A.; Dai, S. Ordered mesoporous polymers for biomass conversions and cross-coupling reactions. *ChemSusChem* **2016**, *9*, 2496–2504. [[CrossRef](#)]
7. Nicolaou, K.C.; Bulger, P.G.; Sarlah, D. Palladium-catalyzed cross-coupling reactions in total synthesis. *Angew. Chem. Int. Ed.* **2005**, *44*, 4442–4489. [[CrossRef](#)]
8. Fang, Y.; Huang, X.J.; Chen, P.C.; Xu, Z.K. Polymer materials for enzyme immobilization and their application in bioreactors. *BMB Rep.* **2011**, *44*, 87–95. [[CrossRef](#)]
9. Khan, M.K.; Giese, M.; Yu, M.; Kelly, J.A.; Hamad, W.Y.; MacLachlan, M.J. Flexible mesoporous photonic resins with tunable chiral nematic structures. *Angew. Chem. Int. Ed.* **2013**, *52*, 8921–8924. [[CrossRef](#)]
10. Inagaki, M.; Toyoda, M.; Soneda, Y.; Tsujimura, S.; Morishita, T. Templated mesoporous carbons: Synthesis and applications. *Carbon* **2016**, *107*, 448–473. [[CrossRef](#)]
11. Jiao, Y.; Han, D.; Ding, Y.; Zhang, X.; Guo, G.; Hu, J.; Yang, D.; Dong, A. Fabrication of three-dimensionally interconnected nanoparticle superlattices and their lithium-ion storage properties. *Nat. Commun.* **2015**, *6*, 6420. [[CrossRef](#)] [[PubMed](#)]
12. Kailasam, K.; Jun, Y.-S.; Katekomol, P.; Epping, J.D.; Hong, W.H.; Thomas, A. Mesoporous melamine resins by soft templating of block-co-polymer mesophases. *Chem. Mater.* **2010**, *22*, 428–434. [[CrossRef](#)]
13. Tanaka, S.; Doi, A.; Nakatani, N.; Katayama, Y.; Miyake, Y. Synthesis of ordered mesoporous carbon films, powders, and fibers by direct triblock-copolymer-templating method using an ethanol/water system. *Carbon* **2009**, *47*, 2688–2698. [[CrossRef](#)]
14. Lu, H.; Shi, Q.; Huang, Z. pH-responsive anionic wormlike micelle based on sodium oleate induced by NaCl. *J. Phys. Chem. B* **2014**, *118*, 12511–12517. [[CrossRef](#)] [[PubMed](#)]

15. Indra, A.; Gopinath, C.S.; Bhaduri, S.; Lahiri, G.K. Hydroxyapatite supported palladium catalysts for Suzuki–Miyaura cross-coupling reaction in aqueous medium. *Catal. Sci. Technol.* **2013**, *3*, 1625–1633. [[CrossRef](#)]
16. Biffis, A.; Centomo, P.; Del Zotto, A.; Zecca, M. Pd metal catalysts for cross-couplings and related reactions in the 21st century: A critical review. *Chem. Rev.* **2018**, *118*, 2249–2295. [[CrossRef](#)] [[PubMed](#)]
17. Liu, F.; Kamat, R.K.; Noshadi, I.; Peck, D.; Parnas, R.S.; Zheng, A.; Qi, C.; Lin, Y. Depolymerization of crystalline cellulose catalyzed by acidic ionic liquids grafted onto sponge-like nanoporous polymers. *Chem. Commun.* **2013**, *49*, 8456. [[CrossRef](#)]
18. Liu, F.J.; Zheng, A.M.; Noshadi, I.; Xiao, F.-S. Design and synthesis of hydrophobic and stable mesoporous polymeric solid acid with ultra strong acid strength and excellent catalytic activities for biomass transformation. *Appl. Catal. B* **2013**, *193*, 136–137. [[CrossRef](#)]
19. Noshadi, I.; Kanjilal, B.; Du, S.; Bollas, G.M.; Suib, S.L.; Provatas, A.; Liu, F.; Parnas, R.S. Catalyzed production of biodiesel and bio-chemicals from brown grease using Ionic Liquid functionalized ordered mesoporous polymer. *Appl. Energy* **2014**, *129*, 112–122. [[CrossRef](#)]
20. Noshadi, I.; Jafari, T.; Kanjilal, B.; Moharreri, E.; Khakpash, N.; Masoumi, A.; Liu, F.; Suib, S.L. Amine/Thiol functionalized mesoporous polydivinylbenzene for CO<sub>2</sub> adsorption. *Mater. Today Energy* **2017**, *4*, 81–88. [[CrossRef](#)]
21. Jafari, T.; Moharreri, E.; Toloueinia, P.; Amin, A.S.; Sahoo, S.; Khakpash, N.; Noshadi, I.; Alpay, A.P.; Suib, S.L. Microwave-assisted synthesis of amine functionalized mesoporous polydivinylbenzene for CO<sub>2</sub> adsorption. *J. CO<sub>2</sub> Util.* **2017**, *19*, 79–90. [[CrossRef](#)]
22. Wang, H.; Jiao, F.; Gao, F.; Huang, J.; Zhao, Y.; Shen, Y.; Zhang, Y.; Qian, X. Facile synthesis of magnetic covalent organic frameworks for the hydrophilic enrichment of N-glycopeptides. *ACS Macro Lett.* **2015**, *4*, 570–574. [[CrossRef](#)]
23. Dupont, J.; Pfeffer, M. *Palladacycles: Synthesis, Characterization, and Applications*; John Wiley & Sons: Hoboken, NJ, USA, 2014; p. 4.
24. Wan, Y.; Wang, H.; Zhao, Q.; Klingstedt, M.; Terasaki, O.; Zhao, D. Ordered mesoporous Pd/Silica–Carbon as a highly active heterogeneous catalyst for coupling reaction of chlorobenzene in aqueous media. *J. Am. Chem. Soc.* **2009**, *131*, 4541–4550. [[CrossRef](#)] [[PubMed](#)]
25. Jin, Z.; Yu, C.; Wang, X.; Wan, Y.; Li, D.; Lu, G. Liquid phase hydrodechlorination of chlorophenols at lower temperature on a novel Pd catalyst. *J. Hazard. Mater.* **2011**, *186*, 1726–1732. [[CrossRef](#)] [[PubMed](#)]
26. Wang, M.; Xue, H.; Ju, F.; Yang, H. Acceleration of batch-type heterogeneous ligand-free Suzuki–Miyaura reactions with polymer composite supported Pd catalyst. *Sci. Rep.* **2017**, *7*, 7006. [[CrossRef](#)] [[PubMed](#)]
27. Jin, T.; Xiong, Z.; Zhu, X.; Mehio, N.; Chen, Y.; Hu, J.; Zhang, W.; Zou, H.; Liu, H.; Dai, S. Template-free synthesis of mesoporous polymers for highly selective enrichment of glycopeptides. *ACS Macro Lett.* **2015**, *4*, 570–574. [[CrossRef](#)]
28. Wan, Y.; Qian, X.; Jia, N.; Wang, Z.; Li, H.; Zhao, D. Direct triblock-copolymer-templating synthesis of highly ordered fluorinated mesoporous carbon. *Chem. Mater.* **2008**, *20*, 1012–1018. [[CrossRef](#)]
29. Yemul, O.; Imae, T. Synthesis and characterization of poly(ethyleneimine) dendrimers. *Colloid Polym. Sci.* **2008**, *286*, 747–752. [[CrossRef](#)]
30. Zhu, L.; Dasgupta, T.; Huang, Q. A D-optimal design for estimation of parameters of an exponential-linear growth curve of nanostructures. *Technometrics* **2014**, *56*, 432–442. [[CrossRef](#)]
31. Dasgupta, T.; Weintraub, B.; Joseph, V.R. A physical–statistical model for density control of nanowires. *IIE Trans.* **2011**, *43*, 233–241. [[CrossRef](#)]
32. Dasgupta, T.; Weintraub, B.; Joseph, V.R. Palladium PEPPSI complexes: Synthesis and catalytic activity on the Suzuki–Miyaura coupling reactions for aryl bromides at room temperature in aqueous media. *Inorg. Chim. Acta* **2018**, *478*, 187–194.
33. Touj, N.; Gürbüz, N.; Hamdi, N.; Yaşar, S.; Özdemir, İ. The palladium(II) complex of N,N-diethyl-1-ferrocenyl-3-thiabutylamine: Synthesis, solution and solid state structure and catalytic activity in Suzuki–Miyaura reaction. *RSC Adv.* **2014**, *4*, 43792–43799.
34. Opanasenko, M.; Stepnicka, P.; Cejka, J. Heterogeneous Pd catalysts supported on silica matrices. *RSC Adv.* **2014**, *4*, 65137. [[CrossRef](#)]
35. Gao, S.; Zhao, N.; Shu, M.; Che, S. Palladium nanoparticles supported on MOF-5: A highly active catalyst for a ligand- and copper-free Sonogashira coupling reaction. *Appl. Catal. A* **2010**, *388*, 196–201. [[CrossRef](#)]

36. Polshettiwar, V.; Luque, R.; Fihri, A.; Zhu, H.; Bouhrara, M.; Bassett, J.-M. Magnetically recoverable nanocatalysts. *Chem. Rev.* **2011**, *111*, 3036–3075. [[CrossRef](#)]
37. Zhang, L.; Wen, G.; Liu, H.; Wang, N.; Su, D.S. Preparation of palladium catalysts supported on carbon nanotubes by an electrostatic adsorption method. *ChemCatChem* **2014**, *6*, 2600–2606. [[CrossRef](#)]
38. Farina, V. High-turnover palladium catalysts in cross-coupling and heck chemistry: A critical overview. *Adv. Synth. Catal.* **2004**, *346*, 1553–1582. [[CrossRef](#)]
39. Groppo, E.; Agostini, G.; Borfecchia, E.; Wei, L.; Giannici, F.; Portale, G.; Longo, A.; Lamberti, C. Formation and growth of Pd nanoparticles inside a highly cross-linked polystyrene support: Role of the reducing agent. *J. Phys. Chem. C* **2014**, *118*, 8406–8415. [[CrossRef](#)]
40. Capka, M.; Hetflejš, J. Hydrosilylation catalysed by transition metal complexes coordinately bound to inorganic supports. *Collect. Czech. Chem. Commun.* **1974**, *39*, 154–166. [[CrossRef](#)]
41. Sharf, V.Z.; Gurovets, A.S.; Finn, L.P.; Slinyakov, I.B.; Krutii, V.N.; Freidlin, L.K. Catalytic activity of metal complexes anchored to a solid support. 2. Synthesis of palladium complexes on amino-containing silica gels and their properties in the hydrogenation of C=C, C≡C, and C=N bonds. *Acad. Sci. USSR Div. Chem. Sci.* **1979**, *28*, 93–96.
42. Alan, R.K. *Advances in Heterocyclic Chemistry*; Acad. Press: Cambridge, MA, USA, 2013; p. 326.
43. Tamami, B.; Farjadian, F.; Ghasemi, S.; Allahyari, H. Synthesis and applications of polymeric N-heterocyclic carbene palladium complex-grafted silica as a novel recyclable nano-catalyst for Heck and Sonogashira coupling reactions. *New J. Chem.* **2013**, *37*, 2011–2018. [[CrossRef](#)]
44. Paul, S.; Clark, J.H. Structure-activity relationship between some novel silica supported palladium catalysts: A study of the Suzuki reaction. *J. Mol. Catal. A Chem.* **2004**, *215*, 107–111. [[CrossRef](#)]
45. Vassilyev, O.; Chen, J.; Panarello, A.P.; Khinast, J.G. Catalytic properties of several supported Pd(II) complexes for Suzuki coupling reactions. *Tetrahedron Lett.* **2005**, *46*, 6865–6869. [[CrossRef](#)]



© 2019 by the authors. Licensee MDPI, Basel, Switzerland. This article is an open access article distributed under the terms and conditions of the Creative Commons Attribution (CC BY) license (<http://creativecommons.org/licenses/by/4.0/>).